Remote Sensing Applications: Society and Environment 18 (2020) 100306

Contents lists available at ScienceDirect

Remote Sensing Applications: Society and Environment

journal homepage: http://www.elsevier.com/locate/rsase

Mapping of ferric $^{(Fe3+)}$ and ferrous $^{(Fe2+)}$ iron oxides distribution using band ratio techniques with ASTER data and geochemistry of Kanjamalai and Godumalai, Tamil Nadu, south India

Gopinathan P [a,*], Parthiban S [b], Magendran T [c], Ayad M. Fadhil Al-Quraishi [d], Ashok K. Singh [e], Pradeep K. Singh [e]

[a] CSIR-Central Institute of Mining and Fuel Research, Ministry of Science & Technology, Govt of India, Ranchi, Jharkhand, 834010, India
[b] Vignan's Foundation for Science Technology & Research (Vignan's University), Guntur, Andhra Pradesh, 522 213, India
[c] Water Resources Department, Public Works Department, State Govt. of Tamil Nadu, Chennai, Tamil Nadu, 600 113, India
[d] Dept of Environmental Engineering, College of Engineering, Knowledge University, Erbil, 44001, Kurdistan, Iraq
[e] CSIR-Central Institute of Mining and Fuel Research, Ministry of Science & Technology, Govt. of India, Dhanbad, Jharkhand, 826015, India

ARTICLE INFO

Keywords:
ASTER
Geochemistry
Iron ore
Band ratio
Correlation
Tamil Nadu
India

ABSTRACT

The iron ores found in Tamil Nadu State, South India, are major varieties that have been confined with banded magnetite quartzite. The occurrence, distribution, and grade of these deposits significantly vary according to their geological structure and geomorphologic control. In this article, presents a novel approach, based on spectral remote sensing and digital processing of ASTER data, to identify and characterize the iron ores of Kanjamalai and Godumalai areas located in Tamil Nadu, India. By analyzing the ASTER images, the abundance of iron oxides including ferric (Fe^{3+}) and ferrous (Fe^{2+}) components was determined. The band ratioing technique, a multiband analysis was used to generate the abundance of iron oxide content in various parts of the study area using different band combinations such as band 2/band 1 (for Fe^{3+}) and band 5/band 3 + band 1/band 2 (for Fe^{2+}). The geochemical analysis is an important part of this work to arrive with the outcome of band ratio techniques to decipher the relationship of the band ratio to the chemical composition of the ore samples. Accordingly, the correlation between the results of the geochemical analysis of the samples collected from the random locations was determined by Pearson's coefficient of correlation (ρ) and compared with the corresponding locations in the abundance image. In addition to ρ, various factors such as mean (μ), variance (σ^2) and corresponding standard deviations (σ) were also analyzed for a comparative analysis. This comparative analysis indicated that most of the samples have considerably high iron oxide content in the locations. Thus, this study shows the possibility of detecting iron oxide content and its spatial distribution by using ASTER satellite images analysis. Hence, from the mapping results, it is evident that the band ratio technique of ASTER images can be used to map and characterize with limited fieldwork and geochemistry.

1. Introduction

The southern part of India is endowed with a variety of minerals. Among these minerals, some are successfully and economically extracted such as fossil fuel and metalliferous and non-metalliferous minerals (GSI, 2006). The state of Tamil Nadu reserves over 500 million tonnes of magnetite with an average grade of 38% iron in the major deposits of Salem, Tiruvannamalai, Dharmapuri, Tiruchirappalli, Namakkal, Villupuram and Perambalur districts GSI, 2006. Among these iron ore deposits, Kanjamalai and Godumalai were selected for exploring iron ores using remote sensing techniques with ground truth verification. Remote sensing based preliminary study on these sites was previously attempted to assess the generic controls of iron ore deposits Gopinathan et al. (2015a,b).

It is erudite that the digitally processed satellite images can be used to locate the assemblages of hydrothermal alteration minerals such as iron minerals, silica, and clay. Abulghasem et al. (2011) studied the integrated data of remote sensing and geophysical data for iron ore exploration. Subsequent image interpretation produces a map of localities or prospect with favorable conditions for mineral deposits Sabins

* Corresponding author.
E-mail addresses: srigopi555@gmail.com, pgopinathan@cimfr.nic.in (G. P).

https://doi.org/10.1016/j.rsase.2020.100306
Received 4 May 2019; Received in revised form 27 February 2020; Accepted 19 March 2020
Available online 26 March 2020
2352-9385/© 2020 Elsevier B.V. All rights reserved.

(1999), Soe et al. (2005), Ramadan et al. (2009), Zhang et al. (2012). By comparing the signatures of known deposits with the unknown deposits by using band ratio combination, new reserves can be identified Ciampalini and Antonielli (2012), Sabreen and Abdelmoneam (2012), El Khidir and Babikir (2013). Yang et al. (1998) proposed a new exploration technique using a novel exploration parameter, i.e., alteration remote sensing anomaly for metallic deposits. Kruse and Prerry (2006) carried any regional mineral mapping by extending a hyperspectral signature using multispectral data. Hyperspectral images with 0.4–2.5 micrometer (VNIR.SWIR) spectral range allow direct identification of minerals using their fully resolved spectral signatures Kruse (1995), Sabins (1999), Magendran et al. (2011), Zhang et al. (2012). Similar studies using ASTER were also carried out for geospatial and geological mapping of iron ore prospective zones (Crosta et al. (2003), Zhang et al. (2007), Salati et al. (2011) and Mishra et al. (2014). Bersi et al. (2016) has attempted a research carried out with Aero gravity and remote sensing observations of an iron deposit in Gara Djebilet, southwestern Algeria, which shows the combination of remote sensing and gravity results helped to evaluate the ore potential of Gara Djebilet and to estimate the tonnage of the iron ore at Gara Djebilet deposits. There are numerous examples of the application of spectral remote sensing techniques in exploring iron ores.Studies related to the iron ore exploration and investigations using the geospatial technologies were attempted by Azizi and Saibi (2015), Azizi et al. (2015), Saadi et al. (2008a,b), Mogren (2017) have given the ample ideologies in mapping techniques of iron ore deposits using remote sensing technologies. Saibi et al. (2018) has furnished the applications of Remote Sensing in Geosciences in a comprehensive manner. These studies are an important source of intent to carry out this present work. Yazdi et al. (2018), successfully attempted a study on alteration mapping for porphyry copper exploration using ASTER and Quick Bird multispectral images and similar studies on hydrothermally altered mineral mapping were studied by Nabilou et al. (2018), Fakhari et al. (2019), Mirko et al. (2019), Zamyad et al. (2019). These works indicate the credibility of using remote sensing datasets for hydrothermally altered mineral mapping. Magendran and Sanjeevi (2014) and Mezned et al. (2010) employed EO–1 Hyperion, Landsat ETM+ and ASTER images and obtained the most reliable mineral detection including iron ore grade estimation. Many successful studies on iron ore grade estimation using spectral sensing and geochemistry (Morais Maria Carolina de et al. (2010), Magendran et al. (2011), Magendran and Sanjeevi (2014), Gopinathan et al. (2015a,b), Sadeghi et al. (2013) encouraged us to attempt this study for Kanjamalai and Godhumalai regions.

This work is intent to decipher the potential of spectral remote sensing and digital processing of ASTER data, to identify and characterize the iron ores of Kanjamalai and Godumalai in terms of its geological and geochemical paradigms. By analyzing the ASTER images, the abundance of iron oxides including ferric (Fe^{3+}) and ferrous (Fe^{2+}) components was determined with the help of band ratioing technique to generate the abundance of iron oxide content in various parts of the study area using different band combinations such as band 2/band 1 (for Fe^{3+}) and band 5/band 3 + band 1/band 2 (for Fe^{2+}).

2. Materials and methods

2.1. Study area

The sites selected for this study are located in the northwestern part of Tamil Nadu state, South India (Fig. 1). The study area is a part of the Archean high-grade granulite-gneissic terrain of South India in Salem, Tamil Nadu and this terrain contains rocks of diverse chemical and mineralogical compositions Reddy and Sashidhar (1989). Kanjamalai and Godumalai are well known banded iron ore deposits (banded magnetite quartzite) in southern granulite terrain in Tamil Nadu Gopinathan et al. (2015). Table 1 describes the location and typical characteristics of the study sites.

2.2. Geological settings

Kanjamalai is one of the well-known banded iron ore formation hills

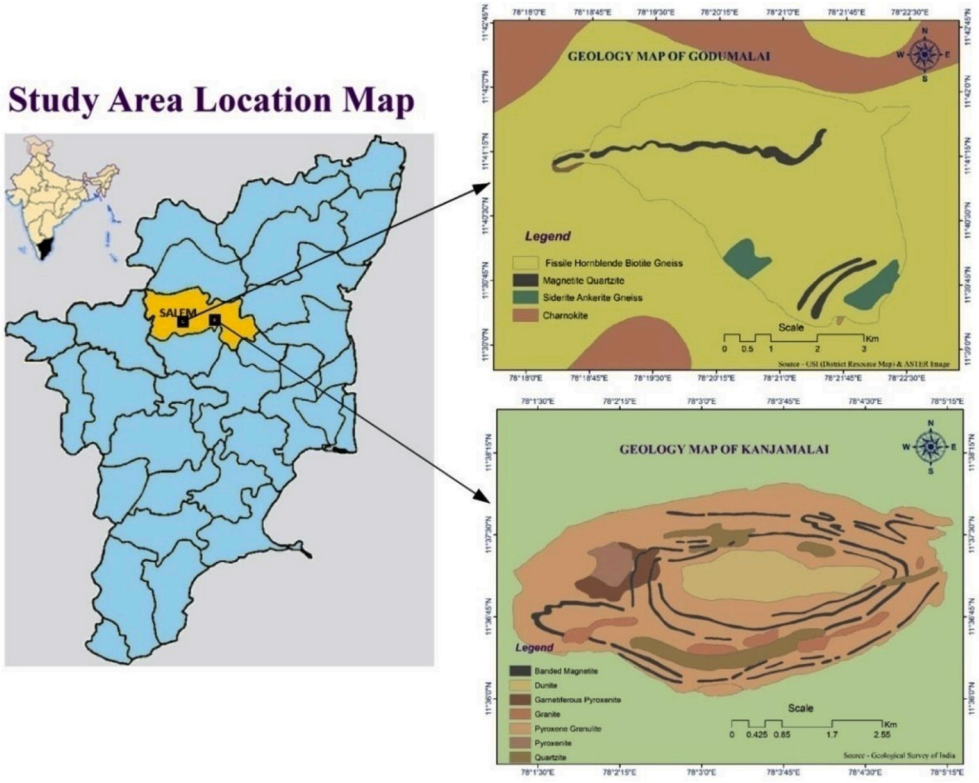

Fig. 1. Showing the key map of the locations and lithology.

Table-1
Results of Geochemical Analysis of all the samples Collected from the Study Sites.

Concentration of Component (%)												
S.No	Sample ID	Al_2O_3	CaO	Fe_3O_4	K_2O	MgO	MnO	Na_2O	P_2O_5	SiO_2	SO_3	TiO_2
1	GS1	1.03	1.324	37.27	0.096	2.002	0.02	0.466	0.372	56.4	0.22	0.04
2	GS2	0.185	1.525	40.12	0.015	2.836	0.01	0.00	0.372	54.9	0.00	0.00
3	GS3	1.346	1.562	36.53	0.085	2.032	0.02	0.521	0.416	54.3	0.16	0.46
4	GS4	0.198	1.136	44.05	0.022	1.864	0.02	0.00	0.324	52.4	0.00	0.00
5	GS5	0.177	1.279	45.47	0.019	2.06	0.02	0.00	0.261	50.7	0.00	0.00
6	GS6	1.54	1.198	39.76	0.15	1.16	0.03	0.492	0.25	57.7	0.25	0.07
7	GS7	17.34	5.193	4.462	2.676	2.797	0.05	6.174	0.224	60.2	0.00	0.51
8	KS1	1.804	0.894	36.9	0.152	1.586	0.05	0.6	0.102	56.8	0.24	0.29
9	KS2	14.37	14.1	12.83	0.05	7.331	0.24	2.64	0.054	47.5	0.00	0.00
10	KS3	1.926	0.586	38.59	0.157	1.491	0.04	0.62	0.278	57	0.31	0.09
11	KS4	0.151	0.52	48.32	0.00	2.203	0.02	0.00	0.401	48.4	0.00	0.00
12	KS5	2.05	3.85	24.92	0.144	1.351	0.03	0.572	0.106	66.3	0.25	0.11
13	KS6	2.14	0.45	50.32	0.16	1.38	0.04	0.461	0.124	45.2	0.18	0.1
14	KS7	2.07	0.728	39.68	0.152	1.24	0.33	0.642	0.153	57.3	0.19	0.21
15	KS8	12.03	16.45	15.44	0.102	8.469	0.22	1.18	0.106	45	0.00	0.81
16	KS9	2.031	0.452	25.02	0.28	1.271	0.24	0.481	0.16	64.8	0.15	0.14
17	KS10	12.97	13.22	13.55	0.107	12.81	0.23	1.74	0.055	44.5	0.00	0.43

(banded magnetite quartzite) in Tamil Nadu, consists of garnet-amphibolite gneiss at top of the hill. Flaggy light-colored gneiss, banded magnetite quartzite (BMQ), massive garnet amphibolite, banded magnetite quartzite (BMQ), hornblendic and feldspathic gneiss, garnet amphibole gneiss, banded magnetite quartzite (BMQ), talcosic schist and light colored flaggy gneiss with and without garnet are present following the order of superposition from the top to bottom of the hill GSI, 2006.

Godumalai hill is situated at a distance of 17.6 km in the east of Salem city. Geologically, the Godumalai banded iron formation that occurs in the top of the hill expands for 4.8 km in the east and west directions (GSI, 2006). Hornblende biotite gneiss covers the entire hill and the lithology of the surrounding area includes amphibolite and pyroxene granulite. The thickness of the ore bands is 3–5 m. A few other bands may exist under the forest cover GSI, 2006. The geological setting of the study sites of Kanjamalai and Godumalai is illustrated in Fig. 1.

3. Methodology

The ASTER (Advanced Spaceborne Thermal Emission and Reflection Radiometer) image data used in this study covering the iron ore deposits of Kanjamalai and Godumalai were acquired in 2001. The ASTER image data spectrally cover the visible and near-infrared radiometer (VNIR), shortwave-infrared radiometer (SWIR), and thermal infrared radiometer (TIR) regions with 14 spectral bands and creates high resolution (15–90 m) multispectral images of the Earth surface (Yamaguchi et al., 2001). ASTER measures reflected radiation in three bands between 0.52 to 0.86 μm (VNIR) and in six bands from 1.6 to 2.43 μm (SWIR) with 15 and 30 m resolution, respectively. ASTER is also equipped with a back-looking VNIR telescope with 15 m resolution; thus stereoscopic VNIR images can be acquired at 15 m resolution. In addition, the emitted radiation is measured at 90 m resolution in five bands in the 8.125–11.65 μm wavelength region (TIR). In this study, VNIR wavelengths were effectively used to decipher the spatial distribution of iron oxide at the studied sites.

The adopted methodology was implemented in three steps: (i) Analysis of remote sensing data (ii) Field investigation and sample collection (ground truth verification), and (iii) Geochemical analysis of the collected samples. In the first step, multispectral image data processing was carried out considering the ASTER satellite datato re-evaluate iron ore deposits. In the second step, a field investigation, based on the output of the remote sensing approach, was conducted and samples were collected. In the third step, geochemical analysis of the collected samples was carried out to verify the predictions made by the remote sensing approach (Fig. 2).The detailed discussions on the analytical results are furnished in the subsequent sections.

4. Results and discussions

4.1. Band selection and ratio analysis

Ratio analysis is used to enhance the spectral contrasts between the bands that are considered in the ratioing process and used in the mineral mapping Elsayed Zeinelabdeina and Albielyb (2008). Each object has its own spectral reflectance pattern in different wavelength regions. The spectral reflectance curve is a kind of fingerprint of an object. The object or rock unit may have high reflectance value in some spectral regions, though it may absorb in another spectral region. For instance, iron ore absorbs in the 0.85–0.9 μm region of electromagnetic radiation (EMR). In this context, the band ratio serves as a simple and powerful technique to identify and demarcate the iron ore mineral deposits. The ferrous mineral abundance maps highlight ferrous (Fe^{2+}) minerals present in an area. The banded magnetite quartzite shows magnetite ridges in the

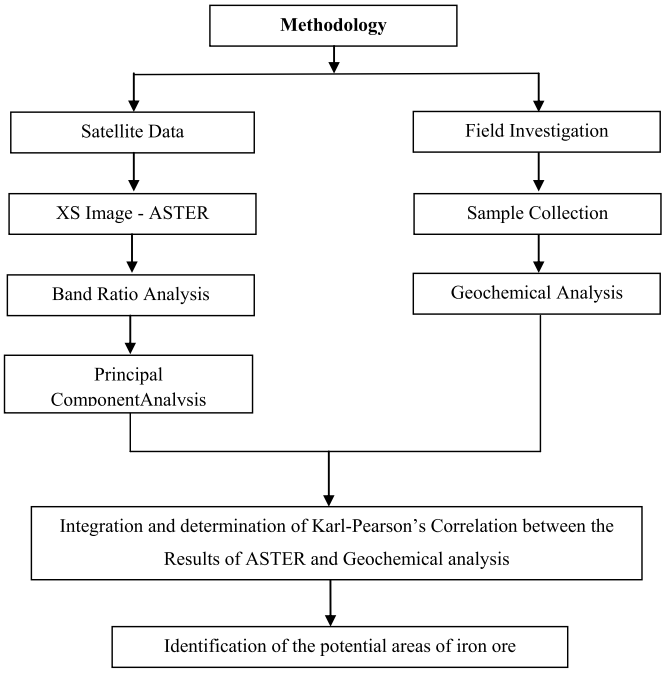

Fig. 2. Flowchart depicting the methodology employed.

visible region of the map.

In a band ratio image, the red, green and blue bands are used for the ratio of any two bands or any arithmetic combination of the bands. Although up to six bands can be considered, in practice, only a few bands are combined in different ways for iteration. Band ratio images are used to remove the effect of uneven illumination caused by the topography with an assumption that the ratio of two bands in the same rock type will be the same, no matter in which way the slope faces.

4.2. Abundance mapping of ferrous mineral

ASTER band 5/3 + band 1/2 ratio was used to generate ferrous mineral abundance map. The ratio images designed to display the spectral contrast of specific absorption features have extensively been used to identify ferrous iron oxides. The ferrous mineral abundance map is used to highlight the ferrous minerals mainly ores of iron in the map. The ASTER band combinations used to prepare the ferrous abundance map included band 5/3 + band 1/2. Fig. 3 depicts the areas of ferrous abundance at the study sites.

Owing to the absorption characteristics displayed by iron oxide in the NIR region, it is possible to map the spatial distribution of ferrous minerals by using an algorithm. Ferrous minerals can be seen mostly in the flanks of slops and the foot hills of Godumalai area. In the Kanjamalai area, they are seen near the ridges and foot of the hills. However, the abundance of ferrous minerals is less in Kanjamalai than that in Godumalai. Certain scattered patches can be seen at ground level but these are mostly red soils and do not correspond to iron mineralization in the region.

4.3. Ferric Mineral Abundance Mapping

The abundance map of iron oxides was generated to highlight ferric minerals. This index map is different from that of the ferrous minerals in such a way that the iron oxide includes all the materials showing red color on the ground. In other words, it includes iron ores, red soils, and laterites. The ASTER band combination used for the preparation of iron oxide abundance map is band 2/band1.

The difference between the abundance map of ferrous and ferric minerals is the oxidation states Fe2+ and Fe3+. The abundance of ferric oxide at the study sites is different and readily depicted in the output image (Fig. 4). On the other hand, in Godumalai, ferric oxide is not abundant, perhaps due to the presence of vegetation on the hill. However, in Kanjamalai, ferric oxide abundance is readily seen at most of the parts of the hill.

4.4. Linear spectral unmixing for grade estimation

Linear spectral unmixing determines the relative abundance of materials depicted in multispectral imagery considering spectral characteristics of materials. The reflectance at each pixel of the image is assumed to be a linear combination of the reflectance of each material (end member) present within the pixel. However, there are certain limitations in applying the linear spectral unmixing technique. The number of end members must be less than the number of spectral bands and all of the end members in the image must be used for an efficient mapping result Kumar et al. (2008). The results of spectral unmixing are highly dependent on the input of end members and changing end members also changes the final results.

4.5. Principal components analysis (PCA)

Different bands in multispectral data are often highly correlated and thus contain similar information. For example, Landsat MSS Bands 4 and 5 (Green and Red, respectively) typically have similar visual appearance since the reflectance for the different types of same surface cover is almost equal. Image transformation techniques can be used to reduce this data redundancy and correlation between bands. One such transform is called principal components analysis. The objective of this transformation is to reduce the dimensionality (i.e., the number of bands) in the data and compress as much as the information in the original bands into fewer bands. The "new" bands that result from this procedure are called components. This process attempts to maximize (statistically) the amount of information (or variance) from the original data into the least number of new components. As an example of the use of principal components analysis, a seven-band Thematic Mapper (TM) dataset may be transformed such that the first three principal components contain over 90 percent of the information in the original seven bands. The interpretation and analysis of these three bands of data can be done easily and more efficiently by combining them both visually or digitally rather than trying to use all original seven bands. Principal components analysis and other complex transforms can be used either as an enhancement technique to improve visual interpretation or to reduce the number of bands to be used as input to information extraction Geological Survey of Canada (2004).

In the end member selection process, the multiple end members were selected to specify the sub-classes of target iron oxide minerals and country rocks each of which representing different combinations of pixel density, pixel size, and percentage cover that lead to the fluctuation in the reflectance value in the spectra. The resulting sub-classes were then combined to obtain the final end member spectra of iron oxide and country rock (Fig. 5). The red and green envelope spectra represent area distributed with iron oxide and white spectra represent different country rocks in the study areas.

4.6. Fraction images

Fraction images were generated by using two end members such as iron oxides and country rocks for the study sites. It shows that higher values are displayed as brighter and lower values are displayed in darker tones for each pixel. This fraction image for the two study sites gives

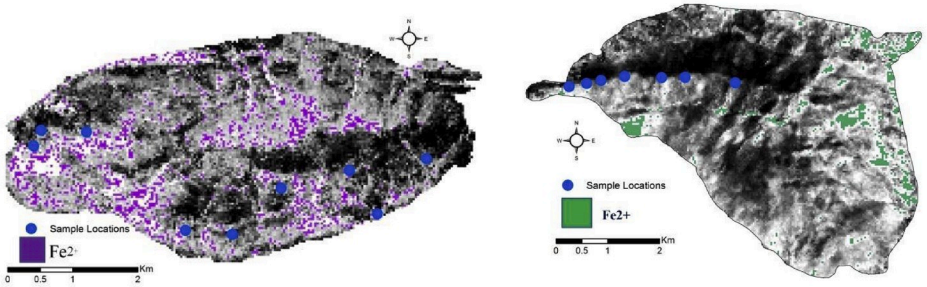

(a) (b)

Fig. 3. Ferrous Mineral Abundance Map of Study sites (a) Kanjamalai and (b) Godumalai.

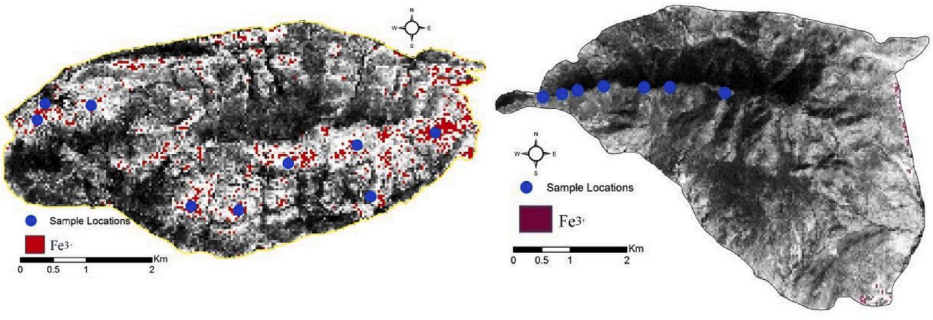

(a) (b)

Fig. 4. Ferric Mineral Abundance Map of Study sites (a) Kanjamalai and (b) Godumalai.

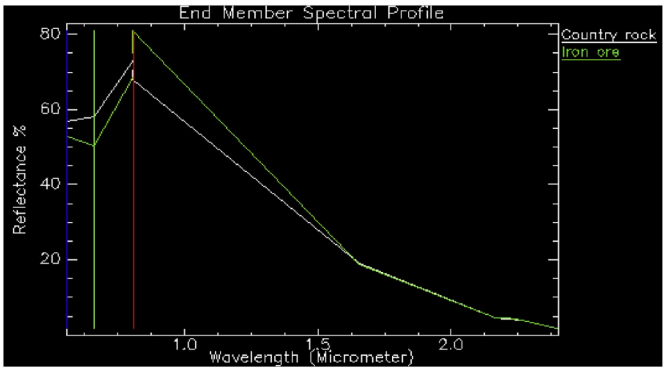

(a)

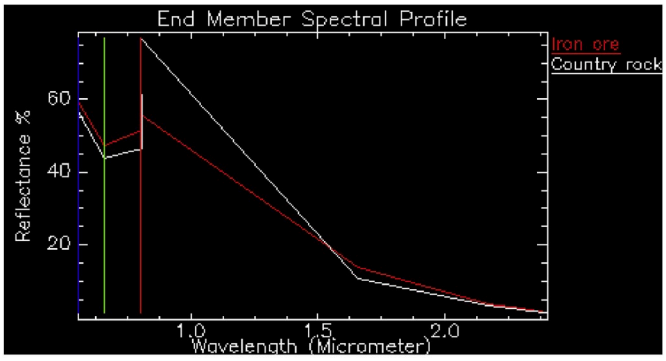

(b)

Fig. 5. End Member Spectra collected for the Study Sites (a) Kanjamalai and (b) Godumalai.

information about the relative abundance of the end member material considering each end member present in a pixel. Two end members for each study site were used to describe the resultant images (Fig. 6).

The fraction images of the study sites clearly indicate the presence of iron oxide minerals and the country rocks. The brighter areas in the fraction images represent higher abundances of the corresponding end member components. Most of the brighter areas in the iron oxide fraction images indicate only the iron ore ridges and the moderate abundance of iron oxide is prominent in slopes of the hill. Similarly, brighter areas in the country rock fraction images represent country rocks such as quartzite, amphibolite, pyroxene granulites, feldspathic gneiss, garnet amphibole gneiss, etc.

4.7. Grade wise categorization mapping of iron ores

Grade wise categorization maps were generated as the iron ore fraction images, which provided iron ore grade variations at the study sites. By density slicing of the fraction images, the iron oxide grades were categorized. Grade wise categorization maps were generated from the iron ore fraction images, since these fraction images provide information about iron ore grade variations in the study sites and thus the categorization was done by density slicing of the fraction images. Density slicing is an image processing technique that is applied to a single-band monochromatic image to highlight the areas appearing uniform in tone. Grey scale values (generally 0 to 255) are converted to a series of specific slices and different colors are assigned to each slice. This technique is often used to highlight variations in vegetation. However, in the present study, the variation in ore grade is highlighted in the fraction images by using this technique.

Thus, the entire data range of a fraction image is selected and sliced into three different categories of classes and represented in different colors. In the output image, the high-grade iron oxide is assigned and represented by the yellow color, the medium grade iron oxide is assigned and represented by the blue color and the low-grade iron oxide is assigned and represented by the green color. This procedure was applied to the fraction images of both study sites. The grade wise categorization map of iron ores based on the abundance is shown in Fig. 7.

It is necessary that the grades of these iron ore pockets estimated by remote sensing are validated and compared with the actual geochemistry of the samples. Hence, the geochemical analysis was carried out to relate the actual geochemistry of the samples and the abundance of the iron ores in the selected locations with high grade, medium grade, and low grade. The next section presents the results of the geochemical analysis of the iron ore samples.

4.8. Sample collection and geochemical analysis

In order to validate the prediction made by remote sensing, field investigation and sample collection were conducted. The ground survey was conducted for field investigation or ground truth verification after processing and analyzing the ASTER image data. Based on the iron ore abundance map, the field verification was done and various sampling locations were identified using a portable global positioning system. A total of 17 samples were collected from various parts of the study sites (Fig. 8) Due care was taken during the sample collection in such a way that the samples fall in the iron ore exposure area, which was identified from the ASTER data process and analysis (see Fig. 9abc).

The geochemical analysis of the samples was aimed to relate the abundance of the iron oxide determined by the satellite data analysis with the actual geochemistry of the collected samples. After collecting iron ore samples during the field investigation and ground truth verification, the samples were powdered to 100-μm size. These powdered samples were prepared for XRF analysis to identify the total iron content

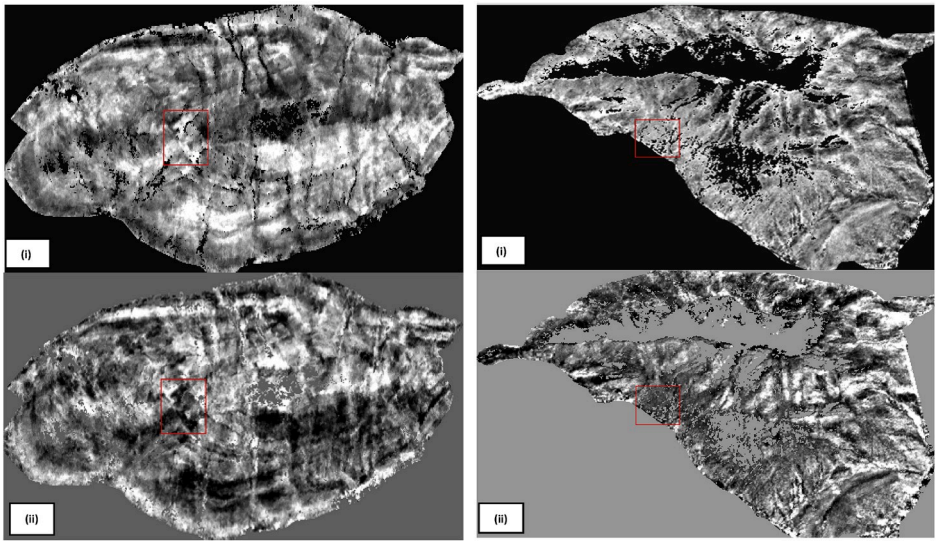

Fig. 6. Fraction images generated for study sites (a) Kanjamalai: (i) Iron ore fraction image; (ii) country rock fraction image and (b) Godumalai: (i) Iron ore fraction image; (ii) country rock fraction image.

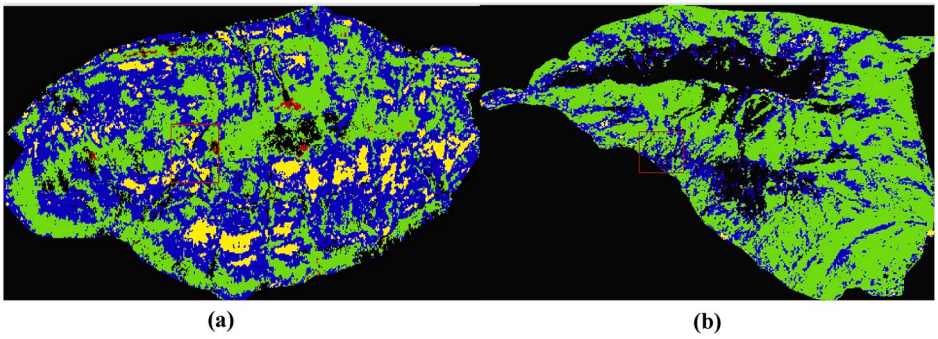

Fig. 7. Grade wise Categorization Map of the Study sites (a) Kanjamalai and (b) Godumalai.

Fig. 8. Field photographs showing banded iron ore formations of the study area.

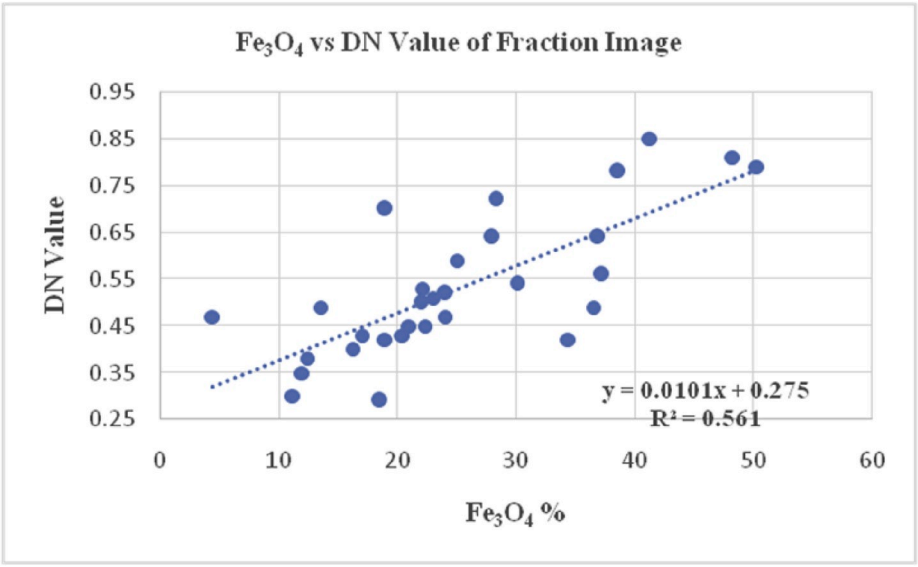

Fig. 9 (a). Correlation between Fe_3O_4 and DN value of fraction image.

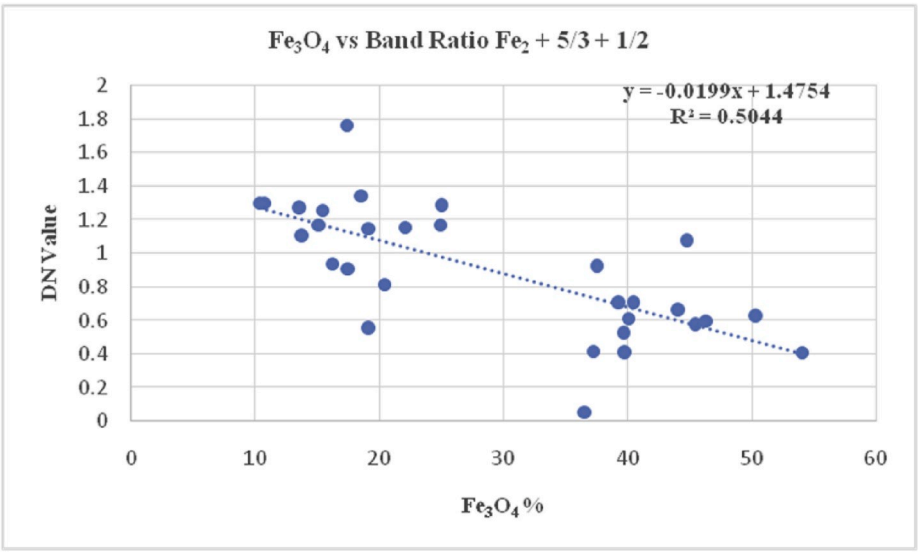

Fig. 9(b). Correlation between the actual iron oxide and band ratio for ferrous oxide ($Fe_2 + 5/3 + 1/2$).

in the samples. The results of geochemical analysis of all the samples are presented in Table 1 - **Table-1. Results of Geochemical Analysis of all the samples Collected from the Study Sites, should come here**.

4.9. Pearson's correlation coefficient between the results of ASTER vs geochemistry

Linear spectral unmixing techniques are useful in categorizing the grade of iron ores based on their abundance. The correlation between the different factors of the collected samples was established by Pearson's correlation coefficient. Besides the correlation analysis, other significant factors were also analyzed and compared for better interpretation. The correlation between the predicted iron oxide abundance and the actual geochemistry of the samples was established by the following equation:

Pearson's correlation coefficient.

$$\rho(x,\ y) = \frac{\mathrm{Cov}(x,\ y)}{\sigma_x \cdot \sigma_y} \quad \text{where} \quad \text{mean} \quad \mu_x = \frac{\sum x}{n}; \quad \text{mean}\mu_y = \frac{\sum y}{n}; \mathrm{Cov}(x,\ y) = \frac{\sum xy}{n} - \frac{\sum x}{n}\cdot\frac{\sum y}{n} \sigma_x = \sqrt{\frac{\sum x^2}{n} - \left(\frac{\sum x}{n}\right)^2} \quad \text{and.} \quad \sigma_y = \sqrt{\frac{\sum y^2}{n} - \left(\frac{\sum y}{n}\right)^2}$$

Where 'n' is the number of items taken for the samples.

Pearson's correlation coefficient for Fe_3O_4 vs. DN value of fraction image

Fe_3O_4 vs. DN value of Fraction Image	
Mean $\mu_{Fe_3O_4} = 25.2455$	Mean $\mu_{\text{Fraction Image}} = 0.5307$
Variance $\sigma^2_{Fe_3O_4} = 119.5369$	Variance $\sigma^2_{\text{Fraction Image}} = 0.0219$
Standard Deviation $\sigma_{Fe_3O_4} = 10.9333$	Standard Deviation $\sigma_{\text{Fraction Image}} = 0.1480$
$\mathrm{Cov}(Fe_3O_4,\ \text{Fraction Image}) = 1.2108$	
$\rho(Fe_3O_4,\ \text{Fraction Image}) = 0.7490$	
$\Rightarrow R^2 = \rho^2 = 0.5610$	

The correlation between the predicted iron oxide abundance versus actual geochemistry is $R^2 = 0.5610$, indicating that there is a good correlation between the ASTER observation and actual geochemistry of

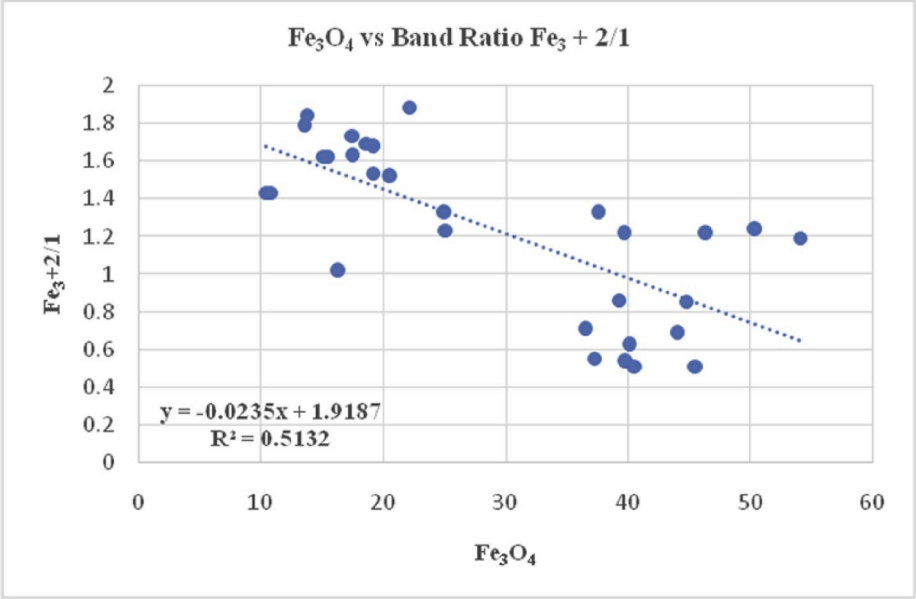

Fig. 9(c). Correlation between Fe_3O_4 and $Fe_3 + 1/2$.

the ore for iron oxide.

Karl-Pearson's correlation coefficient for band ratio Fe_3O_4 vs. $Fe_2 + 5/3 + 1/2$

Fe_3O_4 vs. Band ratio $Fe_2 + 5/3 + 1/2$	
Mean $\mu_{Fe_3O_4} = 29.1595$	Mean $\mu_{Fe_2 + 5/3 + 1/2} = 0.8962$
Variance $\sigma^2_{Fe_3O_4} = 177.9058$	Variance $\sigma^2_{Fe_2 + 5/3 + 1/2} = 0.1392$
Standard Deviation $\sigma_{Fe_3O_4} = 13.3381$	Standard Deviation $\sigma_{Fe_2 + 5/3 + 1/2} = 0.3731$
$Cov(Fe_3O_4, Fe_2 + 5/3 + 1/2) = -3.5340$	
$\rho(Fe_3O_4, Fe_2 + 5/3 + 1/2) = -0.7102$	
$\Rightarrow R^2 = \rho^2 = 0.5044$	

From the above factors the standard deviations of Fe_3O_4 and $Fe_2 + 5/3 + 1/2$ that is $\sigma_{Fe3O4} = 13.3381$ and $\sigma_{Fe_2 + 5/3 + 1/2} = 0.3731$are also comparatively very low in magnitude. The variance of band ratio $Fe_2 + 5/3 + 1/2$, that is, $\sigma^2 = 0.1392$, is considerably less and there is a positive correlation between Fe_3O_4 and $Fe_2 + 5/3 + 1/2$ derived by ASTER.

Pearson's correlation for Band Ratio $Fe_3 + 2/1$ vs Fe_3O_4

Fe_3O_4 vs Band Ratio $Fe_3 + 2/1$	
Mean $\mu_{Fe_3O_4} = 29.1595$	Mean $\mu_{Fe_3 + 2/1} = 1.2340$
Variance $\sigma^2_{Fe_3O_4} = 177.9058$	Variance $\sigma^2_{Fe_3 + 2/1} = 0.1912$
Standard Deviation $\sigma_{Fe_3O_4} = 13.3381$	Standard Deviation $\sigma_{Fe_3 + 2/1} = 0.4372$
$Cov(Fe_3O_4, Average) = -4.1777$	
$\rho(Fe_3O_4, Average) = -0.7164$	
$\Rightarrow R^2 = \rho^2 = 0.5132$	

It can be seen in the above factors that the standard deviations of Band Ratio $Fe_3 + 2/1$ and Fe_3O_4 that is, $\sigma_{Fe_3 + 2/1} = 0.4372$and $\sigma_{Fe_3O_4} = 13.3381$are also comparatively very low in magnitude. The variance of $Fe_3 + 2/1$ that is $\sigma^2 = 0.1912$ is considerably less and there is a reasonable correlation between Fe_3O_4 and fraction image derived by ASTER.

The ratio technique showed a good correlation with the iron oxide content ($R^2 = 0.5044$ and $R^2 = 0.5132$), thus it seems to be an acceptable and reliable technique for iron ore mapping and grade estimation using ASTER images.

5. Conclusion

This study further confirmed that satellite remote sensing technique offers the exploration of a large area in a very short time and at low cost. The spectral remote sensing and digital processing of ASTER images provided useful information about the abundance of iron oxide at the study sites. Band ratioing technique with different band combinations was found to be efficient in estimating the abundance of iron oxide content at the study sites by using band 2/band 1 (for ferric Fe3+) and band 5/band 3 + band 1/band 2 (for ferrous Fe2+) contents. The fraction images that resulted from the technique of spectral unmixing of the ASTER image pertaining to the study sites clearly demarcated the iron oxide mineral and country rock. Most of the brighter areas in the iron oxide fraction images corresponded to the iron ore ridges only and moderate abundance were prominent in the hill slopes. Similarly, the brighter areas in the country rock fraction images represented country rocks such as quartzite, amphibolite, pyroxene granulites, feldspathic gneiss, and garnet amphibole gneiss.

The results of the geochemical analysis of the samples collected from the random locations were correlated and compared with the corresponding locations in the abundance image. The correlation of the iron oxide percentage with the structural pattern confirmed that Godumalai and Kanjamalai have an average of 37.87% and 35.9% of iron oxide content. This further clarified that the banded iron ore formations associated with Godumalai and Kanjamalai are comparatively dominant.

In summary, the current study established that it is possible to detect the narrow and low iron oxide content and quantitatively estimate its spatial distribution using ASTER image data. Moreover, the ratio technique is useful in the identification of the abundance of iron oxide content including lateritic areas. Linear spectral unmixing techniques are useful in categorizing the grade of iron ores based on their abundance with reasonable accuracy. This study demonstrated that using the remote sensing and digital image processing of satellite images such as ASTER, the superficial extension of iron ore deposits can be identified and characterized with limited field works and geochemistry.

Ethical statement for Remote Sensing Applications: Society and Environment

I testify on behalf of co-author that our article submitted to Remote

Sensing Applications: Society and Environment.

Declaration of competing interest

The authors whose names are listed immediately below certify that they have NO affiliations with or involvement in any organization or entity with any financial interest (such as honoraria; educational grants; participation in speakers' bureaus; membership, employment, consultancies, stock ownership, or other equity interest; and expert testimony or patent-licensing arrangements), or non-financial interest (such as personal or professional relationships, affiliations, knowledge or beliefs) in the subject matter or materials discussed in this manuscript. Author names:

Acknowledgement

The authors are thankful to the Director, CSIR-Central Institute of Mining & Fuel Research (CSIR-CIMFR), Dhanbad for his constant encouragement and support to publish this paper. The authors are grateful to the Commonwealth Scientific and Industrial Research Organisation for open sources information for this research and also thankful to different authors whose papers have been referred here.

References

Morais, Maria Carolina de, Martins Junior, Paulo Pereira, Paradella, Waldir Renato, 2011. Multi-scale approach using remote sensing images to characterize the iron deposit N_1 influence areas in Carajas Mineral Province (Brazilian Amazon). Environ. Earth Sci. 66, 2085–2096.

Abulghasem, Y.A., Akhir, J.M., Samsudin, A.R., Hassan, W.F.W., Youshah, B.M., 2011. Integrated data of remote sensing and geophysical data for iron ore exploration in the western part of Wadi Shatti district, Libya. Electron. J. Geotech. Eng. 16, 1441–1454.

Azizi, M., Saibi, H., 2015. Integrating gravity data with remotely sensed data for structural investigation of the Aynak-Logar Valley, eastern Afghanistan, and the surrounding area. IEEE J. Selected Top. Appl. Earth Observa. Rem. Sens. 8 (2), 816–824.

Azizi, M., Saibi, H., Cooper, G.R.J., 2015. Mineral and structural mapping of the Aynak-Logar Valley (Eastern Afghanistan) from hyperspectral remote sensing data and aeromagnetic data. Arab. J. Geosci. 8, 10911–10918.

Bersi, M., Saibi, H., Chabou, M.C., 2016. Aerogravity and remote sensing observations of an iron deposit in Gara Djebilet, southwestern Algeria. J. Afr. Earth Sci. 116, 134–150.

Ciampalini, A., Antonielli, B., 2012. Remote sensing techniques using Landsat ETM+ applied to the detection of iron ore deposits in Western Africa. Arab. J. Geosci. 12517-012-0725-0.

Crosta, A.P., De Souza Filho, C.R., 2003. Targeting key alteration minerals in epithermal deposits in Patagonia, Argentina, using ASTER imagery and principal component analysis. Int. J. Rem. Sens. 24 (21), 4233–4240.

El Khidir, Sami O., Babikir, Ibrahim A.A., 2013. Digital image processing and geospatial analysis of Landsat 7 ETM+ for mineral exploration in Abidiya area, North Sudan. Int. J. Geomatics Geosci. 3 (3).

Elsayed Zeinelabdeina, K.A., Albielyb, A.I., 2008. Ratio image processing techniques: a processing tool for mineral deposits, red sea hills, NE Sudan. Int. Arch. Photogram. Rem. Sens. Spatial Inf. Sci. XXXVII. , Part B8, Beijing 2008.

Fakhari, S., Jafarirad, A., Afzal, P., Lotfi, M., 2019. Delineation of hydrothermal alteration zones for porphyrysystems utilizing ASTER data in Jebal-Barez area, SE Iran. Iran. J. Earth Sci. 11, 80–92.

Geological Survey of Canada, 2004. Rem. Sens. Geosci.

Gopinathan, P., Mohan, S.P., Magendran, T., 2015a. Spectral remote sensing and digital processing of satellite images for characterizing the iron ores of Kanjamalai, Godumalai and Nainarmalai, India - a case study. Int. J. Sci. Res. 4 (4), 3125–3130.

Gopinathan, P., Mohan, S.P., Magendran, T., 2015b. Structural, mineralogical and ore grades of banded iron deposits of north-western Tamilnadu, south India - a comparative study. Int. J. Emerg. Technol. Adv. Eng. 5 (3), 78–83.

Geological survey of India, 2006. Detailed Information Dossier (Did) on Iron Ore in India.

Kruse, Fred A., 1995. Advances in Hyperspectral Remote Sensing for Geologic Mapping and Exploration. Analytical Imaging and Geophysics LLC.

Kruse, Fred A., Perry, Sandra L., 2006. Regional Mineral Mapping by Extending Hyperspectral Signatures Using Multispectral Data. IEEEAC paper #1078, Version 4, Updated. (Accessed 24 November 2006).

Kumar, U., Kerle, N., Ramachandra, T., 2008. Constrained linear spectral unmixing technique for regional land cover mapping using MODIS data. In: Elleithy, K. (Ed.), Innovations and Advanced Techniques in Systems, Computing Sciences and Software Engineering. Springer, Dordrecht.

Magendran, T., Sanjeevi, S., 2014. Hyperion image analysis and linear spectral unmixing to evaluate the grade of iron ores in parts of Noamundi, eastern India. Int. J. Appl. Earth Obs. Geoinf. 26, 413–426.

Magendran, T., Sanjeevi, S., Bhattacharye, A.K., 2011. Hyperspectral radiometry to quantify the grade of iron ore of noamundi and Joda Mines, eastern India. J. Indian Soc Rem. Sens. 39 (4), 473–483.

Mezned, N., Abdeljaoued, S., Boussema, M.R., 2010. A comparative study for unmixing based Landsat ETM+ and ASTER image fusion. Int. J. Appl. Earth Obs. Geoinf. 12, S131–S137.

Mirmohammadi, M., Mirko, A., Afzal, P., Yasrebi, A.B., Carranza, E.J., 2019. Fractal modeling and fry analysis of the relationship between structures and Cu mineralization in Saveh region, Central Iran. Ore Geol. Rev. 107, 172–185.

Mishra, B.K., Pattanayak, S., Rautray, S., 2014. Geospatial and geological mapping of iron ore prospective zones in singbhum keonjhar belt Orissa. Stand. Glob. J. Sci. Res. 1 (1), 0123-019, Feb 2014.

Mogren, S., Saibi, H., Mukhopadhyay, M., Gottsmann, J., Ibrahim, E., 2017. Analyze the spatial distribution of lava flows in Al-Ays Volcanic Area, Saudi Arabia, using remote sensing. Arab J Geosci 10, 133.

Nabilou, M., Arian, M., Afzal, P., Adib, A., Kazemi, A., 2018. Determination of relationship between basement faults andalteration zones in Bafq-Esfordi region, central Iran. IUGS Eposodes J. Int. Geosci. (3), 143–159.

Ramadan, T.M., ElKelani, A.H., Hassaan, M.M., Salem, M.S., 2009. Use of remote sensing and geological studies in the exploration for iron deposits in the oweinat, el Dakhla district, western desert, Egypt. Aust. J. Basic Appl. Sci. 3 (1), 254–266.

Reddy, N.S., Sashidhar, A.N., 1989. Mineralogy and chemistry of banded iron formations (BIF) of Tiruvannamalai area, Tamil Nadu. J. Earth Syst. Sci. 98 (2), 167–172.

Saadi, N., Aboud, E., Saibi, H., Watanabe, K., 2008a. Integrating data from remote sensing, geology and gravity for geological investigation in the Tarhunah area, northwest Libya. Int. J. Digital Earth 1 (No. 4), 347–366.

Saadi, N., Watanabe, K., Imai, A., Saibi, H., 2008b. Integrating potential fields with remotely sensed data for geological investigations in Eljufra area, Libya. Earth Planets Space 60 (No. 6), 539–547.

Sabins, Floyd F., 1999. Remote sensing for mineral exploration. Ore Geol. Rev. 14, 157–183.

Sabreen, G.A.D., Abdelmoneam, R.A.E.F., 2012. Factor analysis approach for composited ASTER band ratios and wavelet transform pixel-level image fusion: lithological mapping of the NeoproterozoicWadi Kid area, Sinai, Egypt. Int. J. Rem. Sens. 33 (5), 1488–1506.

Sadeghi, B., Khalajmasoumi, M., Afzal, P., Moarefvand, P., Yasrebi, A.B., Wetherelt, A., Foster, P., Ziazarifi, A., 2013. Using ETM+ and ASTER sensors to identify iron occurrences in the Esfordi 1:100000 mapping sheet of Central Iran. J. Afr. Earth Sci. 85, 103–114.

Saibi, H., Bersi, M., Mia, M.B., Saadi, N.M., Al Bloushi, K.M.S., Akavian, R.W., 2018. Applications of remote sensing in Geosciences. In: Hung, M.-C., Wu, Y.-H. (Eds.), Recent Advances and Applications in Remote Sensing Book, Intech Edition, ISBN 978-953-51-5564-5, pp. 181–203 (Chapter 9).

Salati, S., van Ruitenbeek, F.J.A., van der Meer, F.D., Tangestani, M.H., van der Werff, H., 2011. Lithological mapping and fuzzy set theory: automated extraction of lithological boundary from ASTER imagery by template matching and spatial accuracy assessment. Int. J. Appl. Earth Obs. Geoinf. 13 (5), 753–765.

Soe, M., Kyaw, T.A., Takashima, I., 2005. Application of Remote Sensing Techniques on Iron Oxide Detection from ASTER and Landsat Images of Tanintharyi Coastal Area, Myanmar: Scientific and Technical Reports of Faculty of Engineering and Resource Science, vol. 26. Akita University, pp. 21–28.

Yamaguchi, Y., Fujisada, H., Tsu, H., Sate, I., Watanable, H., Kate, M., Kudoh, M., Kahlc, A.B., Pnicl, M., 2001. Aster Early image evaluation. Adv. Space Res. 28 (1), 69–76.

Yang, Jianmin, Zhang, Yujun, Wu, Hua, Deng, Gang, Li, Mengwen, 1998. New Exploration Developments Using a New Exploration Parameter (Alteration Remote Sensing Anomaly) for Metallic Deposits in East Tianshan in their book (Chapter 14)-13.

Yazdi, Z, Rad, J.A., Aghazadeh, M., Afzal, P., 2018. Alteration mapping for porphyry copper exploration using ASTERand QuickBird multispectral images, sonajeel prospect, NW Iran. J. Indian Soc. Rem. Sens. 46, 1581–1593.

Zamyad, M., Afzal, P., Pourkermani, M., Nouri, R., Jafari, M.R., 2019. Determination of hydrothermal alteration zones using remote sensing methods in Tirka area, Toroud, NE Iran. J Indian Soc Rem. Sens.Arab. J. Geosci.IEEE J. Selected Top. Appl. Earth Observ. Rem. Sens.Arab. J. Geosci. 47, 1817–1830, 2019.

Zhang, X., Pazner, M., Duke, N., 2007. Lithologic and mineral information extraction for gold exploration using ASTER data in the south Chocolate Mountains (California). ISPRS J. Photogrammetry Remote Sens. 62 (4), 271–282.

Zhang, B., Wu, Di, Zhang, L., Jiao, Quanjun, Qingting, L., 2012. Applications of hyperspectral remote sensing for environment monitoring in mining areas. Environ. Earth Sci. 65, 649–658.